A novel methodology for affecting the strain paths during hydraulic bulge tests by means of laser heat treatments

A. Cusanno, D. Carty, G. Palumbo

PII: S0997-7538(25)00003-8

DOI: https://doi.org/10.1016/j.euromechsol.2025.105569

Reference: EJMSOL 105569

To appear in: *European Journal of Mechanics / A Solids*

Received Date: 3 September 2024

Revised Date: 17 December 2024

Accepted Date: 6 January 2025

Please cite this article as: Cusanno, A, Carty, D., Palumbo, G., A novel methodology for affecting the strain paths during hydraulic bulge tests by means of laser heat treatments, *European Journal of Mechanics / A Solids*, https://doi.org/10.1016/j.euromechsol.2025.105569.

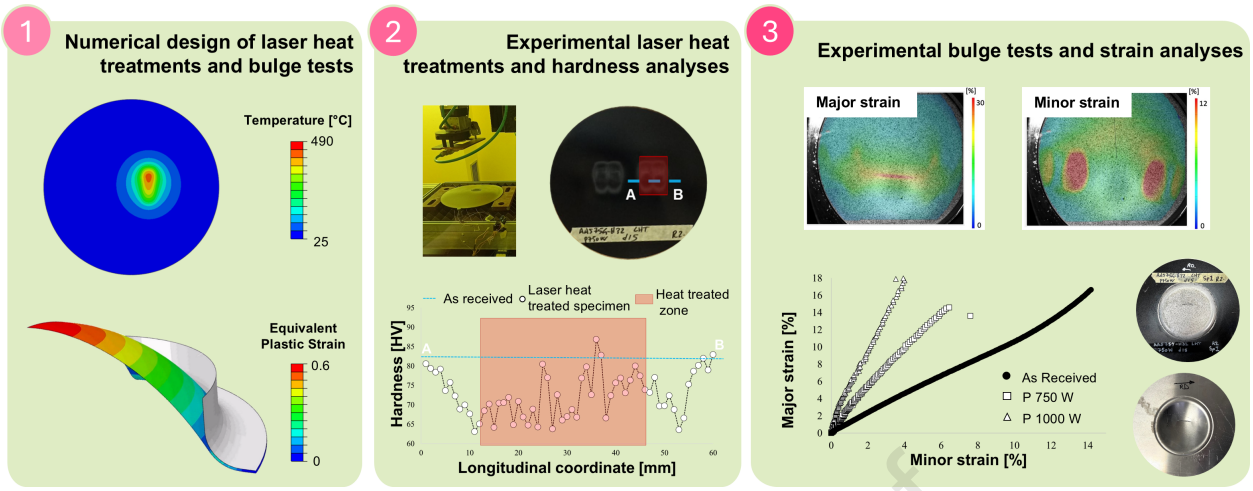

A novel methodology for affecting the strain paths during hydraulic bulge tests by means of laser heat treatments

A.Cusanno[a*], D. Carty[b], G. Palumbo[a]

[a]*Dept. of Mechanics, Mathematics and Management, Politecnico di Bari, Via Orabona 4, 70125 Bari, Italy*

[b]*Advanced Forming Research Centre, University of Strathclyde, 85 Inchinnan Drive, Renfrew PA4 9LJ, United Kingdom*

* *angela.cusanno@poliba.it*

Abstract

Nowadays, the design of manufacturing processes is supported by numerical simulations, that require an understanding of the material forming limits under the process conditions. The hydraulic bulge test represents an effective and well-established experimental procedure to evaluate critical strains of a material. However, it relies on using different elliptical die geometries to vary strain paths, introducing limitations in experimental flexibility. This work aims to evaluate the feasibility of achieving different strain paths during hydraulic bulge tests only using a circular die, by pre-softening certain zones of the testing blank using laser heating. The laser heat treatments (LHTs) were designed using a numerical/experimental approach. Two LHT strategies using different laser power values were performed to locally modify the material properties. Then, hydraulic bulge tests were conducted on the LHTed specimens and the resulting strain paths were analysed. The strain paths acquired during hydraulic bulge tests confirmed the possibility to affect the slope of the strain path at the dome by changing the LHT strategy, designed with the proposed methodology.

Keywords: Laser heat treatment; bulge test; strain path; Digital Image Correlation; AA5754; FE simulation.

1. Introduction

Sheet metal forming (SMF) processes play a crucial role in various industrial sectors, ranging from automotive to aerospace engineering [1,2]. Finite element (FE) simulation is a useful tool to design SMF processes [3]. The ability of the FE models to correctly predict the material behaviour during the forming process strictly depends on the accuracy of the material properties and forming limits implemented in the software. One of the most adopted failure criteria is represented by the Forming Limit Diagram (FLD), that provides a graphical representation of the material formability [4,5]. The transition from safe to failure zones is defined by the forming-limit curve (FLC), that contains the couple of major and minor strains resulting in necking failure considering linear strain paths [6]. In the recent years, new methods have been developed to consider that complex shapes are now produced through multiple stage deformation processes [7]. These path-independent criteria are based on a polar diagram of the effective plastic strain (PEPS-FLD) and the effectiveness of these emerging methods was assessed using different ductile damage criteria as well as different yield models [8–10].

Nakajima and Marciniak methods are two standardised methods to obtain several points on the FLC [11]. These methods involve the use of a punch that deform the material until fracture occurs. Even though these methods are still widely used, their main disadvantage is represented by the friction at the sheet/punch interface, that should be reduced as much as possible also with suitable lubrication systems, since it can alter the test results [12].

An alternative to the above-mentioned methods is the bulge test, which uses a flexible medium to deform the blank instead of a rigid punch. The flexible medium can be a gas for testing hot forming conditions [13,14] or a liquid (e.g., oil [15], water emulsion [16] or smart materials [17,18]) when dealing with lower temperatures. Bulge testing consist of a circular sheet clamped between a circular die and blank-holder; when a pressure is applied to the flexible medium, the sheet is bulged into the cavity of the die

[19]. The main advantage of this approach is that the flexible medium allows to avoid friction effects [20,21], thus being more reliable. The conventional hydraulic bulge test using a die with a circular hole allows to obtain information about material formability in the biaxial stretching condition. However, using elliptical dies with different aperture ratios, different ratios between major and minor strains can be obtained in the range of positive minor strains [20,22,23]. This approach requires the manufacturing of a certain number of dies to obtain the different strain paths. Recently, Banabic et al. [24] proposed a methodology for obtaining different strain paths during hydraulic bulge tests using a cylindrical die, and blanks having two holes with a suitable geometry and position, thus obtaining failure point from tensile to biaxial stretching conditions. The method proposed by Banabic et al. was adopted by Mirnia et al. [15] to reproduce even the in-plane shear state of an AA6061-T6 aluminum alloy sheet. However, to avoid oil leakages from the specimen holes a carrier sheet was required, implying that results may be affected by friction. Oil leakages during hydraulic bulge tests can be avoided only if there are no holes in the testing material. Therefore, another way to achieve different strain conditions on the sheet is needed. One promising method to obtain a local variation of mechanical properties is represented by localised heat treatments [25], following the so-called tailored heat treated blank (THTB) approach [26]. There are several ways to conduct local heat treatments. The most common methods are heating by induction [27], conduction [28] and laser irradiation [29]. Heating using laser irradiation offers low setup and adjustment as well as the localised heating and has proven to be advantageous for the local treatments [26,30]. However, the high thermal conductivity of aluminium alloys represents a significant challenge to effectively conduct the heat treatment using laser radiation; in fact, ensuring enough energy to soften the material must be balanced with the need to localise the treated region and limiting the heat transition zone [31]. To conduct an effective Laser Heat Treatment (LHT), the main process parameters of the holding time, cooling time and the maximum temperature must be properly controlled [32]. Numerical simulation represents a powerful tool to design the LHT parameters and predict the final distribution of

the material properties after the localised heat treatment if properly calibrated [33]. Pereira et al. [34] proved the capability of a LHT to soften critical zones of an advanced-high strength steel (AHSS), obtaining a complex shaped multi-forming industrial part. Piccininni et al. [35] and Fröck et al. [36] determined the optimal laser parameters for locally heat treating an age hardenable aluminium alloy (AA6082) for improving the limit drawing ratio during a deep drawing process and to enhance the formability in bending processes, respectively. Lattanzi et al. [37] studied the LHT applied to a strain hardenable aluminium alloy (AA5754-H32) and they found that, keeping constant the holding time, the softening of the material was strictly connected to the maximum temperature reached by the heat treated zones.

This study introduces a novel approach that involve laser heat treatments to locally modify the material properties in specific zones of the test blanks, using only a circular die. According to the proposed approach, strain paths during hydraulic bulge tests are affected without the need for holes or additional carrier sheets. First, the formability of the alloy AA5754-H32 was investigated; FE simulations of the hydraulic bulge tests were conducted to determine suitable zones to be softened by the local laser treatment; the laser treatment was designed using a numerical/experimental approach. Experimental laser heat treatments were then performed to locally modify the test sample material properties and finally hydraulic bulge tests were conducted on the LHTed specimens and the resulting strain paths were analysed. By combining the flexibility of using only a circular die with the elimination of issues such as oil leakage and friction effects, this approach offers a more reliable test methodology.

2. Materials and Methods

2.1 The alloy investigated.

The alloy investigated was an Aluminium Alloy (5754-H32), having a thickness of 1.5 mm and Vickers Hardness of 85±3 HV. Its chemical composition is reported in Table 1.

Table 1 Chemical composition of the investigated alloy (AA5754-H32)

Si	Fe	Cu	Mn	Mg	Cr	Zn	Ti	Others
0.26	0.38	0.07	0.19	3.1	0.02	0.03	0.02	Balanced

2.2 Design of the laser heat treatments

2.2.1. FE model for simulating hydraulic bulge tests

The hydraulic bulge tests were numerically simulated using Abaqus software, using an implicit time integration scheme. Considering the geometry symmetry, only one quarter of the setup was reproduced, as shown in Figure 1a, thus simplifying the numerical model.

The effect of the drawbead was modelled by constraining the radial displacement and the rotation of the blank's periphery. The die cavity and the blank were modelled as a discrete rigid body and a deformable shell, respectively; in particular, a 4-node, quadrilateral, stress/displacement shell element with reduced integration and a large-strain formulation (S4R) having an average size equal to 0.5 mm were used and five through-thickness integration points were set for the blank. A linear increase of the fluid pressure on the bottom surface of the sheet was set, following the experimental tests. The occurrence of failure was predicted by adopting the FLD damage initiation criterion. Both the stress-strain curve and the Forming Limit Curve (FLC) for the AA5754-H32 sheets were obtained by means of a previous experimental campaign conducted by the authors [38]. By implementing the FLC in the numerical model, a damage based output variable (FLDCRT) was calculated during the simulation. Such a variable is defined as the ratio of the calculated major strain to the major strain on the FLC corresponding to the same minor strain. The model predicted rupture when the FLDCRT variable exceeded the threshold value of 1.

To simulate the effect of the laser heat treatment on the mechanical properties of the base material (ASR), each test sample was modelled partitioning the sheet. As shown in Figure 1b, each sheet was

characterised by three different regions: (i) *LHT*, i.e., the laser heat treated zone, characterised by the mechanical properties of the Al alloy in the annealed condition, (ii) *ASR*, i.e., the base material zone, characterised by the mechanical properties of the Al alloy in the as received condition and (iii) *TZ*, the transition zone, modelled with an offset equal to 2.5 mm from the LHT zone, having intermediate mechanical properties between the LHT and the ASR zones. The LHT zone was characterised by a specific height, *H* (which in the FE model corresponded to the half of it, *H/2*) a specific length, *L*, and a specific distance of the laser track from the centre of the sheet, *d*. The sheet was partitioned to ensure that a structured meshing strategy could be applied to all zones (ASR, LHT, TZ). Neither a remeshing strategy nor meshing optimisation was adopted, since a mesh with a constant average size of 0.5 mm was used.

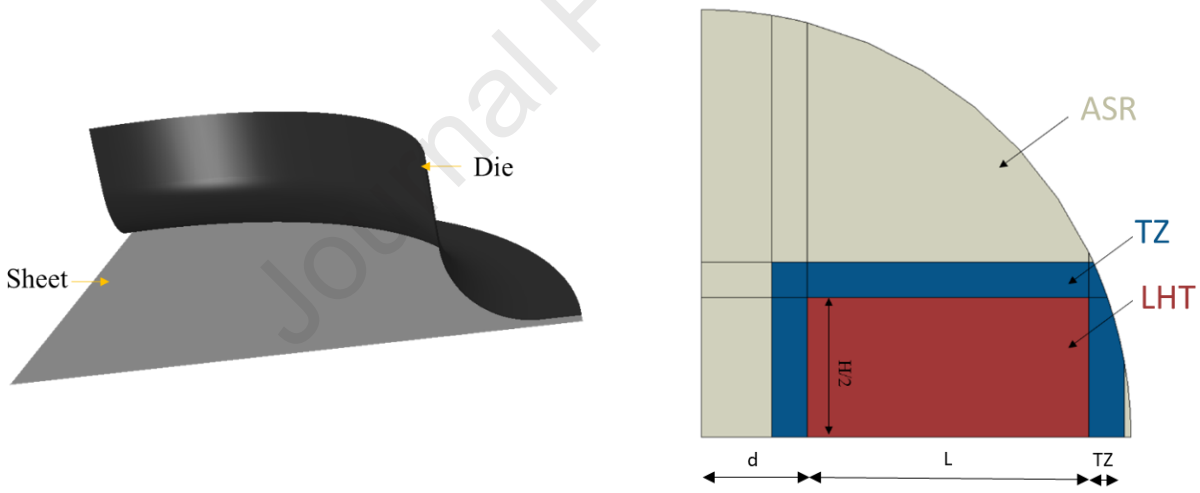

(a) (b)

Figure 1 (a) Assembly used in the numerical model; (b) Overview of the sheet partitioning

Different degrees of annealing were explored from fully annealed condition (100%) and intermediate degrees of annealing (i.e., 25%, 50%, 75%). Thus, different mechanical behaviours (in terms of stress-strain curve) were assigned depending on the degree of annealing set in the LHT region.

The plastic flow behaviour of the material was modelled by fitting experimental data concerning the fully annealed and the wrought condition to evaluate the constant of the Hollomon power law ($\sigma = K * \varepsilon^n$, being σ the true stress, ε the true strain, n the strain-hardening exponent and K the strength coefficient). Then, three intermediate conditions were obtained by linearly interpolating the material constants (K and n) of the fully annealed and the as received material. Table 2 shows the material properties in terms of material constants (K and n) and Yield Stress values adopted for simulating the base material (H32), fully annealed material (H111) and intermediate levels of annealing (i.e., 25%, 50%, 75%).

Table 2 Constant of the Hollomon power law (K and n) and Yield Stress adopted for simulating the base material (H32), fully annealed material (H111) and intermediate levels of annealing (i.e., 25%, 50%, 75%)

Level of annealing [%]	***K* [MPa]**	***n***	**Yield Stress [MPa]**
100 (H111)	384	0.23	117
75	382	0.20	137
50	380	0.17	157
25	378	0.14	177
0 (H32)	376	0.11	197

The strain path at the dome apex was evaluated to assess the effect of the degree of annealing of the LHTed zone on the strain path at the dome of the base material. In the subsequent experimental laser heat treatments, the different degrees of annealing were obtained by adjusting the laser parameters (i.e., laser power, interaction time).

2.2.2. FE model for simulating the laser heat treatment

The laser heating was simulated using the Abaqus software. The evolution of properties was modelled according to the general heat transfer equation:

$$\rho c\dot{T} + div(q) - Q = 0 \qquad (1)$$

Where the heat flux vector q was calculated as $-k \nabla T$ according to the Fourier's law. Density (ρ = 2700 kg/m^3), specific heat (c = 960 J/kg K) and thermal conductivity (k = 147 W/m K) were taken from literature [40]. The value assigned to Q, which is the heat produced by phase transformation, was assumed equal to zero since the material remained solid during laser heating. The power density (I) was defined according to equation 2:

$$I_{eq} = \frac{\eta P}{S} \qquad (2)$$

being η the absorption coefficient, P the laser power set in the experiment, and S the surface covered by the laser beam. To calibrate the absorption coefficient in the thermal model, the adopted squared specimen (100 mm x 100 mm) is shown in Figure 2a. The specimen was modelled as a 3D deformable body and meshed with 20000 hexahedral solid elements (DC3D8) characterised by an approximate global size of 1 mm.

A stationary heat flux was applied to the squared laser spot area (20 mm x 20 mm) located at the centre of the sheet. A simulation plan was run varying the absorption coefficient and considering the temperature evolution over time of the central point (*P1* in Figure 2a) as output. The numerical results were then compared with the experimental curves to determine the correct value of η. The obtained value was used in the FE thermal model for the simulation of the LHT on circular specimens to be successively tested using the hydraulic bulge tests.

The circular bulge specimen (Figure 2b) having a diameter equal to 250 mm was modelled as a 3D deformable body and discretised by average-sized elements of 1 mm (30436 hexahedral DC3D8 solid elements).

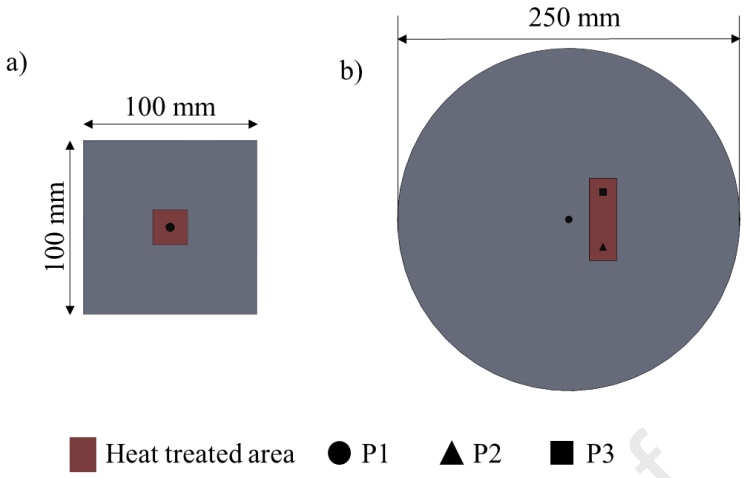

Figure 2 Position of the points for temperature monitoring in the simulations (a) for the calibration FE thermal model and (b) for the laser heat treatments of the circular specimens.

To simulate the laser movement along the defined path and to set the square laser beam profile with a uniform distribution of energy (as in the experimental tests), a specific subroutine (DFLUX) was created. Temperature and time evolution of three specific points were considered as outputs, which are shown in Figure 2b: the first and the second (*P1* and *P2*) corresponding to the starting and ending point of the third laser track (see Figure 3 in Section 2.3), the third one (*P3*) corresponding to the centre of the sheet.

2.3 Experimental Laser Heat Treatments

Laser heat treatments were performed using the 2.5 kW CO_2 laser source shown in Figure 3a. The setup comprised of a heat treatment head moving along the vertical (z) axis, equipped with a Diffractive Optical Element (DOE) to obtain a top-hat energy distribution over a 20 mm square spot, and a working table moving along the remaining two (x&y) axes. The selected LHTed regions on the circular specimens were characterised by a length (L) of 40 mm and a height (H) of 60 mm, being placed symmetrically with a distance (d) of 15 mm from the centre of the sheet. Four linear tracks of heat treatment perpendicular to the rolling direction (RD) were performed using the 20 mm spot, as shown in Figure 3b. In the same figure, the order the tracks were applied to reduce distortions and avoid any non-symmetric heat fluxes

is shown. According to FE simulation results (See Section 3.2), 200 seconds occurred between each laser track. Before the laser heating, one side of the blank facing the laser beam was sprayed with a thin layer of black paint to increase the energy absorbed. All laser heat treatments were characterised by a laser speed of 4 mm/sec. Additionally, two levels of laser power were adopted, 750 W and 1000 W, to explore different levels of annealing. Each condition was repeated three times. Two of the three samples were then tested using hydraulic bulge testing and the third was used to assess the effectiveness of the localised heat treatment by microhardness testing. Vickers microhardness tests were performed along the thickness direction in accordance with the EN ISO 6507-1:2018 standard on a fully automatic Qness microhardness tester. For each condition, Vickers microhardness (load=200 gf, holding time = 15 s) was measured along two different sections: one close to the end of the laser tracks (Section A-B in Figure 3c) and the other close to the starting points (Section C-D). For each section, three different microhardness paths along the thickness direction were analysed, indicated by the *Upper path*, *Middle path* and *Lower path* in Figure 3d. For each path, 60 points at 1 mm from each other were analysed. To ensure that the heat treatment didn't alter the mechanical properties of the base material in the centre of the sheet numerical simulations were performed before the experiments, as reported in Section 2.2.2. To calibrate the FE thermal model, preliminary tests were conducted setting stationary heating on the central zone of the squared specimen and a dwell time equal to 4 seconds, as shown in Figure 3e.

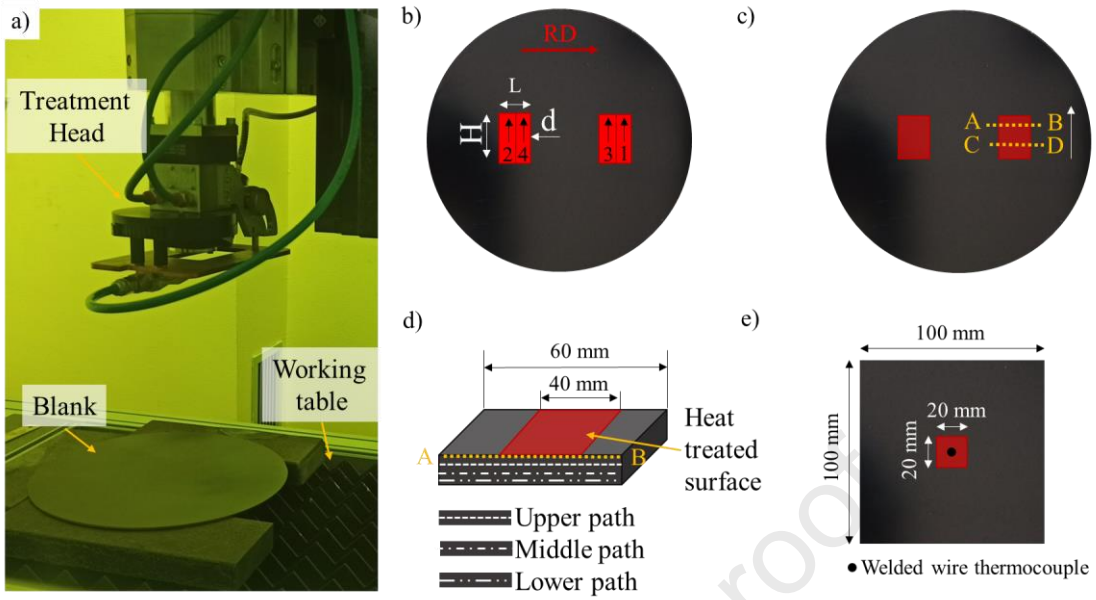

Figure 3 a) Setup for the experimental laser heat treatments; b) detail of the 4 laser tracks c) analysed paths during microhardness tests; d)Detail of the measured hardness paths along thickness direction ; e) Main dimensions of the squared specimen used for the FE numerical model calibration.

During the tests, the temperature evolution according to time of the central point was acquired by means of two 0.25 mm K-type wire thermocouples welded to the specimen's surface on the side not irradiated by the laser beam.

2.4 Experimental hydraulic bulge tests

Figure 4 shows the experimental setup adopted for conducting hydraulic bulge tests. A Zwick-Roell BUP1000 machine equipped with a digital image correlation (DIC) based system (ARAMIS by GOM) was used. It consists of a die (entry radius equal to 10 mm) with a cavity radius of 55 mm, a blank sheet (radius equal to 125 mm), and a blankholder with drawbeads located at a radial position of 14.5 mm far from the die cavity.

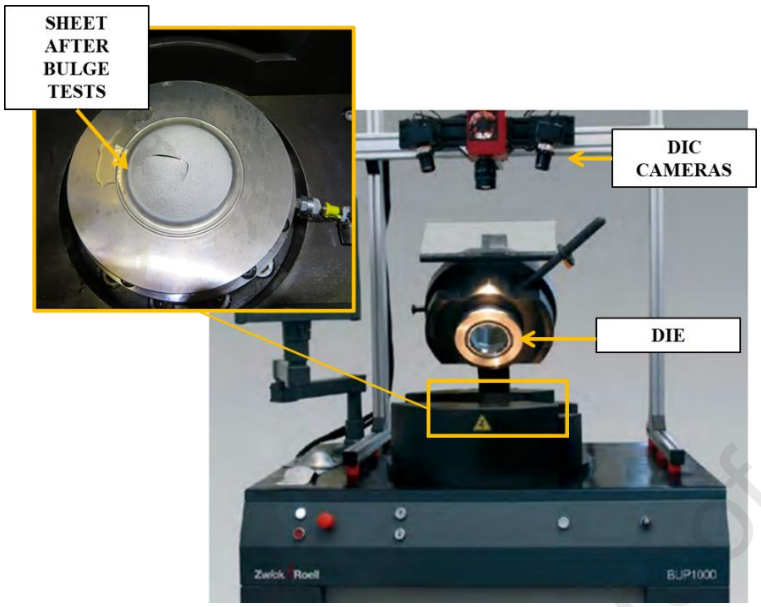

Figure 4 AFRC Zwick-Roell BUP1000 equipment

Before each test, the test samples were prepared with a stochastic speckled pattern. During the tests, the continuous strain acquisition and dome apex was recorded using the DIC system.

3. Results and discussion

3.1 Design of the heat treatment using the FE model

To determine the required size of the annealed zone, preliminary FE simulations were performed to evaluate the effect of the parameters (i.e., the length *L*, height *H* and distance of the laser track from the centre of the sheet *d*), on the strain path at the dome apex. Previous works by the authors [38] evidenced a strong influence of the parameter "d" on the resulting strain path.

Thus, further simulations were performed varying the distance from the centre ranging from 15 mm to 40 mm (i.e., d=15, 20, 30 and 40 mm). For such conditions, mechanical properties corresponding to the fully annealing were assigned to the LHTed zone. Then, the strain path at the dome apex and the FLDCRT map were obtained from numerical simulations to assess the most suitable geometry for the

subsequent experimental laser heat treatments. The resulting strain paths are shown in Figure 5a. It can be noted that reducing the distance from the centre moves the strain paths towards the major strain axis. Additionally, in Figure 5b the corresponding FLDCRT maps are shown.

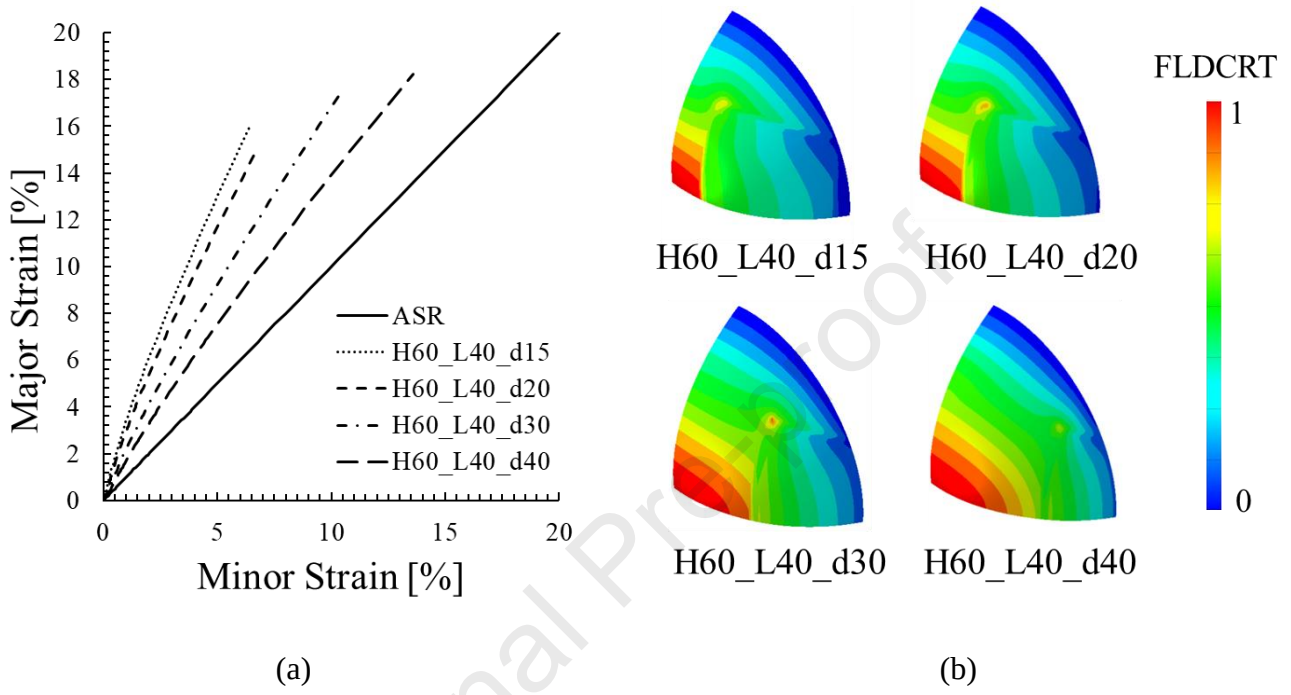

Figure 5 Numerical results: a) Strain paths and at the dome b) FLDCRT map for bulge test simulation of specimens with different distances between the heat treated zones and the centre of the sheet

It can be noted that the lower the distance from the centre, the more localised the fracture. Therefore, a configuration characterised by a distance from the centre equal to 15 mm was chosen.

Figure 6 shows the strain paths at the dome resulting from the simulations using the selected geometrical parameters (L=40 mm, H=60 mm, d=15 mm) and changing the degree of annealing of the LHTed zones. It can be noted that when the degree of annealing was increased, the strain paths moved towards the major strain axis. More in details, the achievable range spans from a slope of 1, corresponding to the strain path of the non-heat-treated specimen (represented by a solid line in Figure 6), to a slope of 2.6, corresponding to the specimen with fully annealed LHTed zones (represented by a dotted line in Figure 6), covering approximately 24°.

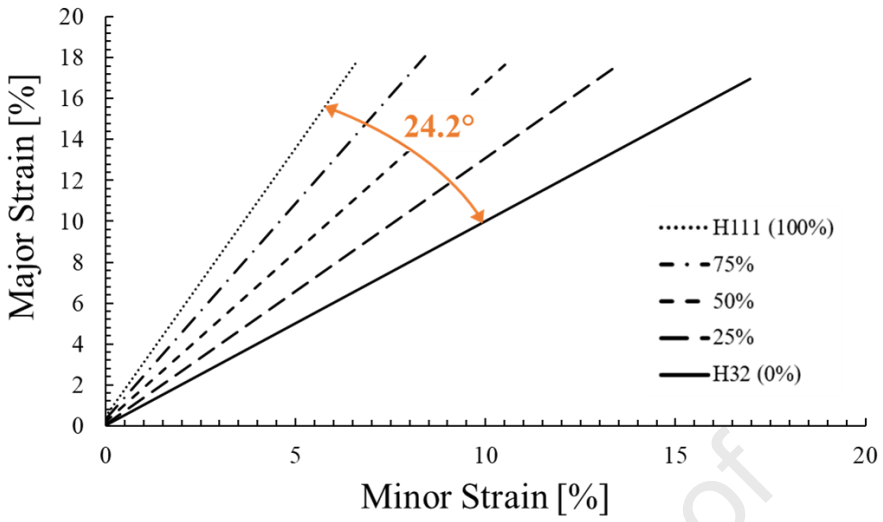

Figure 6 Numerical results of the strain path at the dome using the same geometrical parameters (L=40mm, H=60 mm, d=15mm) and changing the degree of annealing of the LHTed zones

3.2 Simulation of the heat treatment

To calibrate the laser absorption coefficient η, results from the FE thermal model were compared to the temperature acquired by thermocouples at the centre of the blank during the lased heat treatment (Section 2.2.2). The numerical and experimental results concerning the tests in which the laser power was set to 750 W and 1000 W have been shown in Figure 7a and Figure 7b, respectively.

The tuning of the FE model obtained an absorption coefficient η equal to 0.54. Such a FE thermal model could be thus used for simulating the laser heat treatment on circular specimens and to check if the heat treatment is able to alter the mechanical properties of the base material in the centre of the sheet. For this reason, only the third track was numerically simulated, since it was an internal track (i.e., close to the central point).

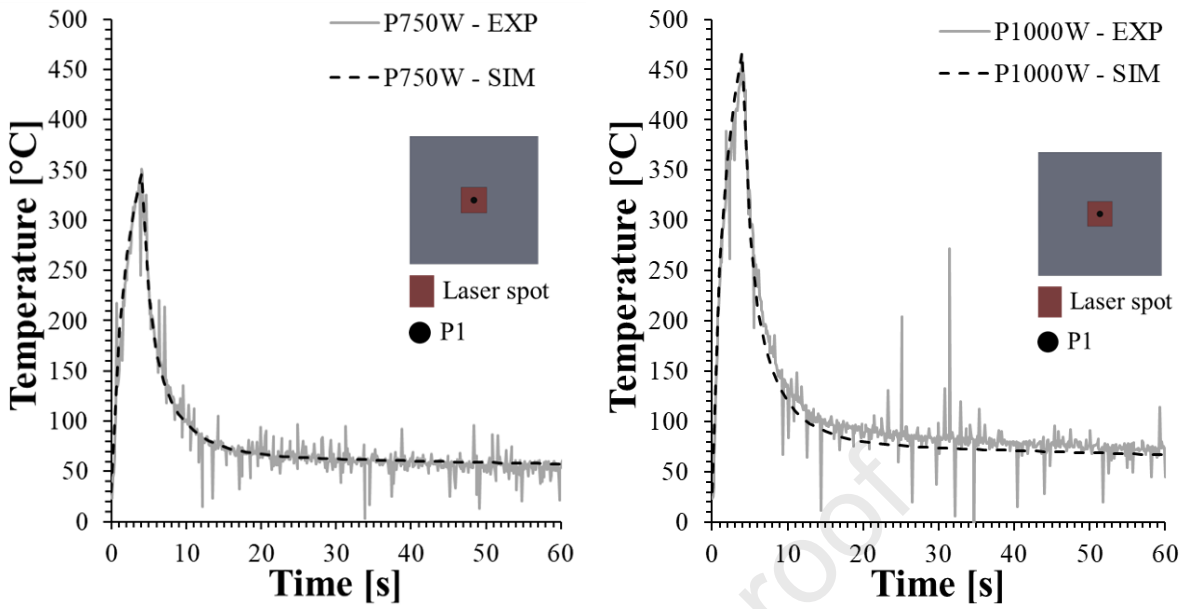

(a) (b)

Figure 7 Numerical/Experimental comparison of the temperature evolution of the central point (P1) during the laser heat treatment for the LHT conducted using (a) P=750W and (b) P=1000W

Figure 8 shows the temperature distribution experienced by the sheet during the LHT. In particular, Figure 8a and Figure 8b show the temperature distribution over time of the three key points (P1 and P2 corresponding to the starting and ending point of the third laser track and P3 corresponding to the centre of the sheet), whereas Figure 8c shows the temperature map of the maximum temperature reached by each node during the LHT.

In the case of the LHT conducted using P=1000W (Figure 8b,c), it can be noticed that the maximum temperature reached on the heat treated areas ranged from 400 °C to 500 °C, whereas the maximum temperature experienced by the centre of the sheet was 120 °C, therefore ensuring that the LHT didn't affect the centre of the sheet [41].

On the other hand, in the case of the LHT conducted using P=750W (Figure 8a, and c), the temperatures reached much lower values, ranging from 340 °C to 430 °C. In this case, the maximum temperature at the centre of the sheet was even lower (100 °C).

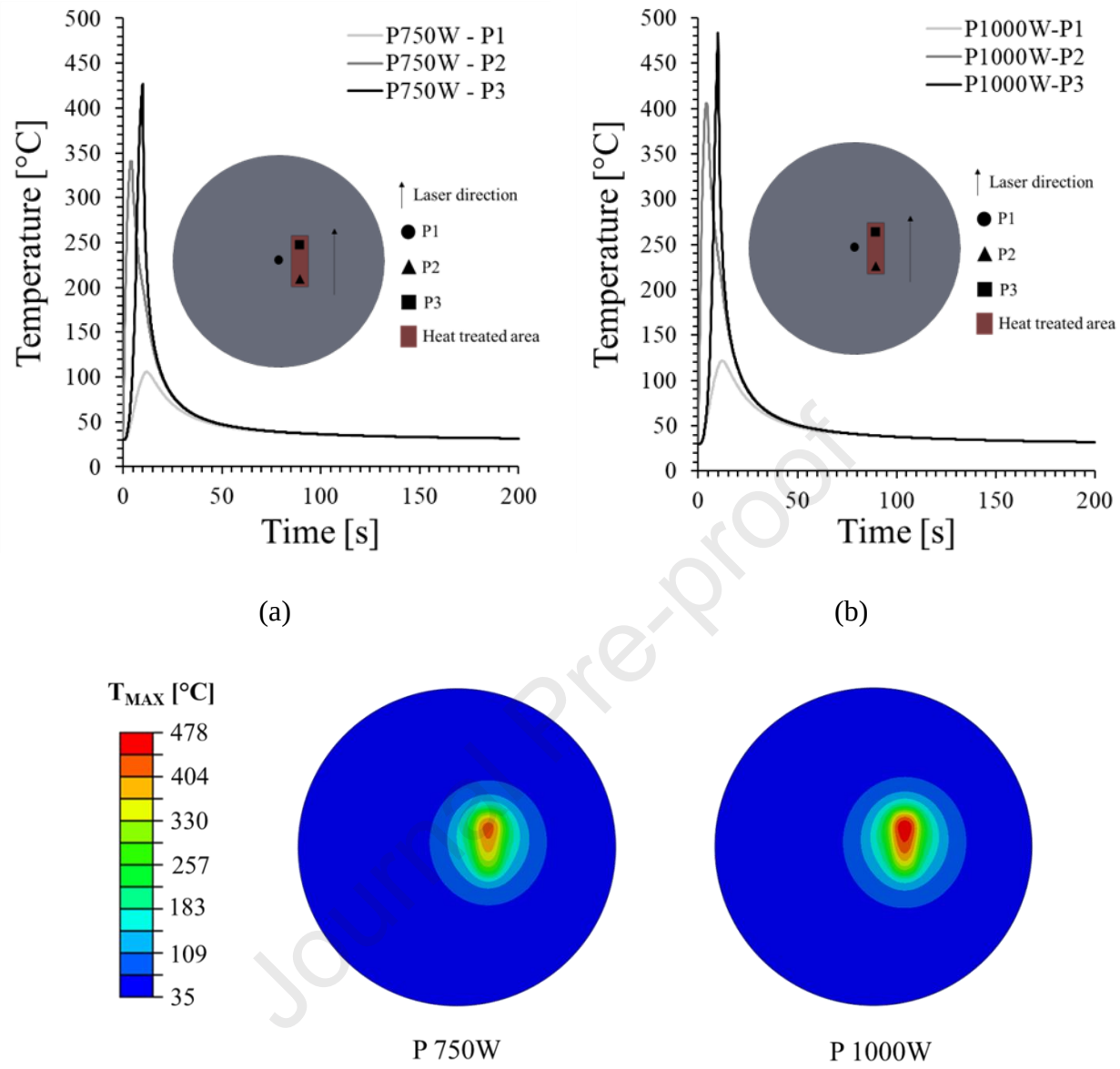

Figure 8 Numerical temperature evolution over time of the three key points (P1 and P2 corresponding to the starting and ending point of the third laser track and P3 corresponding to the centre of the sheet during the laser heat treatment for the LHT conducted using (a) P=750W and (b) P=1000 (c) Temperature map of the maximum temperature reached by each node during the LHT FE simulation

3.3 Experimental results

3.3.1 Hardness measurement of the LHTed samples

Figure 9 gives an overview of the LHTed specimens (for each condition, one of the three samples was used to assess the effectiveness of the localised heat treatment by means of microhardness tests).

Figure 9 Overview of the LHTDed samples

In particular, Figure 10 shows the hardness evolution along the analysed paths of the specimen treated using P=1000W.

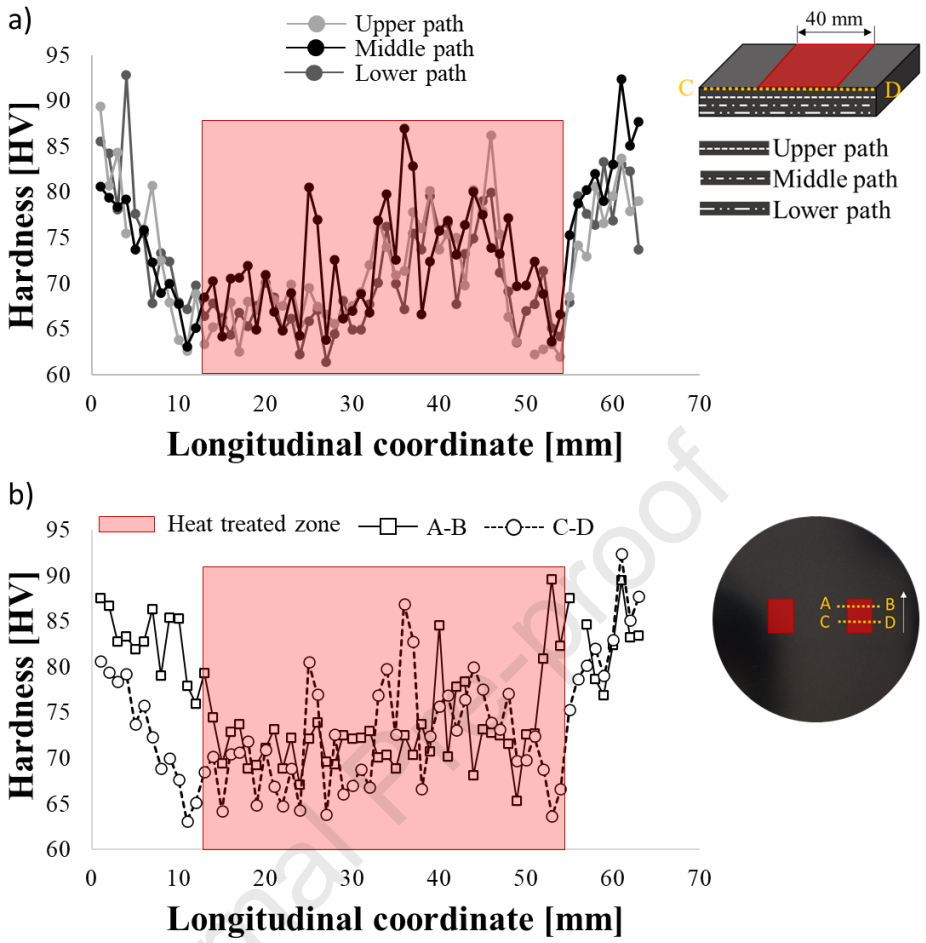

Figure 10 a) Comparison between hardness evolution along the upper, middle and lower path, for the C-D section (P=1000 W); b) Comparison between hardness evolution along the middle path, for both A-B and C-D sections (P=1000 W)

A more detailed comparison between hardness evolution along the Upper, Middle and Lower path, for the C-D section, is shown in Figure 10a. Small differences in hardness values along the thickness direction were noted. Therefore, for the comparison between hardness evolution for A-B and C-D sections, only the middle path was considered (Figure 10b).

From the figure, hardness values in the LHT zone were lower than the base material, suggesting that the combination of laser parameters could alter the material properties in the desired zones. In particular, the average value in the LHTed zone is 69.4±1.9 HV, i.e., 18% lower than the starting hardness.

3.3.2 Strain path evolution of the LHTed samples

Figure 11 shows the major and minor strain maps obtained using the DIC system corresponding to the last image acquired before the rupture both on the *ASR* (Figure 11 a, b) and a *LHT* (Figure 11 c, d) test samples (a laser Power of 1000 W was used for the LHT).

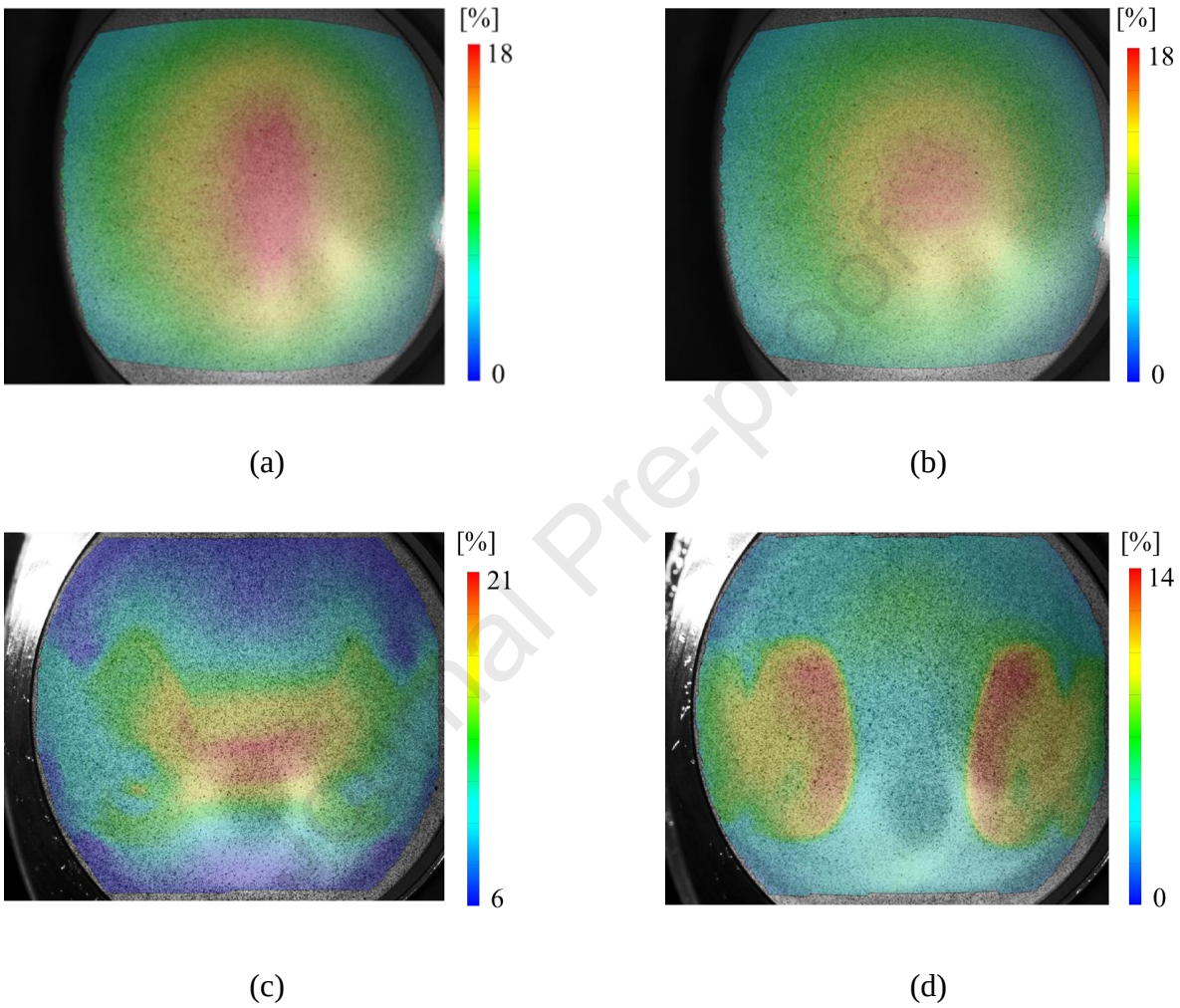

Figure 11 a) Major and b) Minor Strain maps before rupture obtained using the DIC Aramis system for the As Received specimen and c) Major and d) Minor Strain maps before rupture obtained for the treated using a Power of 1000 W (R2)

For the *ASR* specimen, the typical strain distribution cab be recognised, i.e., both the maximum value of major (Figure 11 a) and minor strain (Figure 11 b) occurred in the dome area.

On the other hand, for the *LHTed* specimens, the major strain map (Figure 11 c) reveal that the maximum values of major strain are concentrated in the dome area as in the *ASR*, whereas the maximum values of

minor strain are located in the heat treated zones. The described behaviour is representative for all the heat treated specimens, thus confirming the effectiveness of using the heat treated regions to produce different strain states, by promoting the material deformation in the minor strain direction [5].

Figure 12 shows the comparison between the strain paths at the dome. It emerges that laser heat treatment has led to a significant increase in the slope of the curves compared to the test on the *ASR* specimen. Additionally, it is worthy of notice that the slope of the strain path increased according to the power level which, in turn, affected the temperature experienced by the material in the heat treated zone.

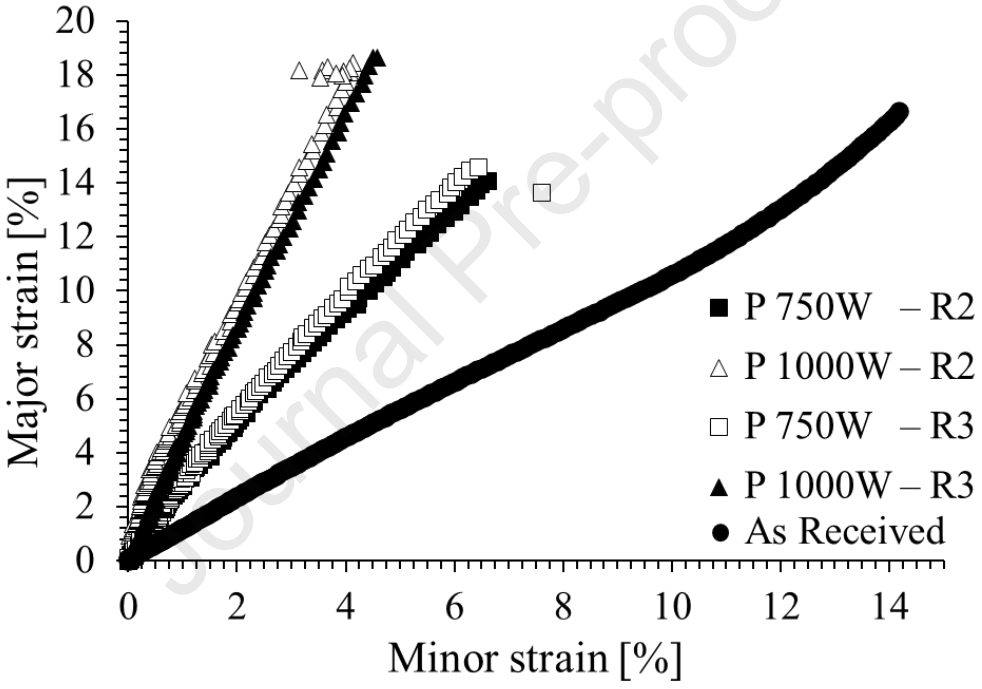

Figure 12 Strain path at the dome for the LHTed and the as received specimens.

More in detail comparison revealed the average slope of the specimen treated using a Power equal to 750 W was 2.24 and it increases up to 4.27 in the case of the P1000W compared to the *ASR* specimen, slope of 1 (experiencing an equi-biaxial stretching strain state). This means that by changing the LHT strategy, it is possible to obtain different intermediate stretching strain states on the dome height of the tested sheet samples. The limitation of this approach is similar to that of conventional hydraulic bulge tests: the range of achievable strain paths is restricted to the right-hand side of the forming limit diagram.

Conclusions

In this work, a novel methodology for affecting the strain paths during hydraulic bulge tests by means of laser heat treatments in specific areas was proposed. The attention was focused on the aluminium alloy an AA5754-H32, but the proposed methodology can be extended to any material whose properties can be modified by means of a heat treatment.

The main achievements can be summarised as follows:

- Through the simulation of the bulge test, it was possible to evaluate the target distribution of properties, the way they may influence the slope of the strain path and determine suitable zones to be heat treated;
- Through the thermal simulations the laser treatment could be designed and the laser power able to affect the centre of the sheet (i.e., the dome apex where the strains are monitored during the hydraulic bulge tests) could be determined;
- The strain paths acquired during bulge tests confirmed the possibility of affecting the slope of the strain path at the dome by changing the LHT strategy.

Future works will be aimed at implementing the outputs coming from the thermal FE model into the mechanical one to speed up the design of the heat treatment procedure, as well as expanding the proposed approach to different alloys.

Acknowledgments

Financed by the European Union - NextGenerationEU (National Sustainable Mobility Center CN00000023, Italian Ministry of University and Research Decree n. 1033 - 17/06/2022, Spoke 11 - Innovative Materials & Lightweighting). The opinions expressed are those of the authors only and should not be considered as representative of the European Union or the European Commission's official position. Neither the European Union nor the European Commission can be held responsible for them.

The authors also wish to thank Dr. Antonio Piccininni and Dr. Pasquale Guglielmi for their support in the numerical and experimental activities.

References

[1] Du Z, Wang C, Liu Q, Wang S, Liu Y, Wang G. The superplastic forming/diffusion bonding of TA7 titanium alloy for manufacturing hollow structure with stiffeners. J Manuf Process 2022;73:385–94. https://doi.org/10.1016/j.jmapro.2021.10.064.

[2] Bell C, Corney J, Zuelli N, Savings D. A state of the art review of hydroforming technology Its applications, research areas, history, and future in manufacturing n.d. https://doi.org/10.1007/s12289-019-01507-1/Published.

[3] Ablat MA, Qattawi A. Numerical simulation of sheet metal forming: a review. International Journal of Advanced Manufacturing Technology 2017;89:1235–50. https://doi.org/10.1007/s00170-016-9103-5.

[4] Bouziane K, EL Mrabti I, Touache A, Chamat A, EL Hakimi A, Moujibi N. Numerical prediction and experimental validation of forming limit curves of laminated half-hard aluminum sheets. International Journal of Advanced Manufacturing Technology 2024. https://doi.org/10.1007/s00170-024-13473-3.

[5] ISO 12004-2:2021 2021.

[6] Banabic D, Bunge H-J, Pöhlandt K, Tekkaya AE. Formability of Metallic Materials. Berlin, Heidelberg: Springer Berlin Heidelberg; 2000. https://doi.org/10.1007/978-3-662-04013-3.

[7] Stoughton TB, Yoon JW. Path independent forming limits in strain and stress spaces. Int J Solids Struct, vol. 49, 2012, p. 3616–25. https://doi.org/10.1016/j.ijsolstr.2012.08.004.

[8] Basak S, Panda SK. Implementation of Yld96 anisotropy plasticity theory for estimation of polar effective plastic strain based failure limit of pre-strained thin steels. Thin-Walled Structures 2018;126:26–37. https://doi.org/10.1016/j.tws.2017.04.015.

[9] Basak S, Panda SK. Necking and fracture limit analyses of different pre-strained sheet materials in polar effective plastic strain locus using Yld2000-2d yield model. J Mater Process Technol 2019;267:289–307. https://doi.org/10.1016/j.jmatprotec.2018.10.004.

[10] Basak S, Panda SK. Use of uncoupled ductile damage models for fracture forming limit prediction during two-stage forming of aluminum sheet material. J Manuf Process 2023;97:185–99. https://doi.org/10.1016/j.jmapro.2023.04.042.

[11] Hou Y, Myung D, Park JK, Min J, Lee HR, El-Aty AA, et al. A Review of Characterization and Modelling Approaches for Sheet Metal Forming of Lightweight Metallic Materials. Materials 2023;16. https://doi.org/10.3390/ma16020836.

[12] Cai G, Wu C, Gao Z, Lang L, Alexandrov S. Research on Al-alloy sheet forming formability during warm/hot sheet hydroforming based on elliptical warm bulging test. AIP Adv 2018;8:55023. https://doi.org/10.1063/1.5029539/920608.

[13] Boyer A, Demazel N, Coër J, Carin M, Laurent H, Oliveira MC. A novel hydraulic bulge test in hot forming conditions. J Mater Process Technol 2023;316. https://doi.org/10.1016/j.jmatprotec.2023.117917.

[14] Sorgente D, Palumbo G, Scintilla LD, Tricarico L. Gas forming of an AZ31 magnesium alloy at elevated strain rates. International Journal of Advanced Manufacturing Technology 2016;83:861–72. https://doi.org/10.1007/s00170-015-7614-0.

[15] Mirnia MJ, Vahdani M. Calibration of ductile fracture criterion from shear to equibiaxial tension using hydraulic bulge test. J Mater Process Technol 2020;280. https://doi.org/10.1016/j.jmatprotec.2020.116589.

[16] Öztürk O, Korkmaz HG, Ataş G, Aydin M, Türköz M, Toros S, et al. Formability improvement in Ti–6Al–4 V sheet at room temperature by pulsating hydraulic bulging: experimental and numerical investigations. International Journal of Advanced Manufacturing Technology 2023;124:2903–18. https://doi.org/10.1007/s00170-022-10693-3.

[17] Wang ZJ, Wang PY, Song H. Research on sheet-metal flexible-die forming using a magnetorheological fluid. J Mater Process Technol 2014;214:2200–11. https://doi.org/10.1016/J.JMATPROTEC.2014.04.016.

[18] Cusanno A, Piccininni A, Guglielmi P, Palumbo G. Evaluation of the Rheological Behaviour of Magnetorheological Fluids Combining Bulge Tests and Inverse Analysis. Key Eng Mater, vol. 926 KEM, Trans Tech Publications Ltd; 2022, p. 1778–85. https://doi.org/10.4028/p-4irh1n.

[19] ISO 16808:2022 - Metallic materials — Sheet and strip — Determination of biaxial stress-strain curve by means of bulge test with optical measuring systems n.d. https://www.iso.org/standard/82103.html (accessed April 3, 2024).

[20] Lăzărescu L, Comşa DS, Nicodim I, Ciobanu I, Banabic D. Characterization of plastic behaviour of sheet metals by hydraulic bulge test. Transactions of Nonferrous Metals Society of China 2012;22:s275–9. https://doi.org/10.1016/S1003-6326(12)61719-1.

[21] Wang P yi, Xiang N, Wang Z jin, Li Z xin. The rapid response of forming medium's properties to variable loading types of magnetic field and consequent field-dependent sheet formability. J Manuf Process 2018;31:468–79. https://doi.org/10.1016/J.JMAPRO.2017.12.006.

[22] Williams BW, McKinley J, Boyle KP, Blaga L, Kurukuri S, Worswick MJ. Warm Forming Response of ZEK100 Sheet obtained under Biaxial Stretching with Full-Field Displacement Measurements. IOP Conf Ser Mater Sci Eng, vol. 418, Institute of Physics Publishing; 2018. https://doi.org/10.1088/1757-899X/418/1/012030.

[23] Banabic D, Balan T, Comsa DS. Closed-form solution for bulging through elliptical dies. J Mater Process Technol 2001;115:83–6. https://doi.org/10.1016/S0924-0136(01)00773-7.

[24] Banabic D, Lazarescu L, Paraianu L, Ciobanu I, Nicodim I, Comsa DS. Development of a new procedure for the experimental determination of the Forming Limit Curves. CIRP Annals 2013;62:255–8. https://doi.org/10.1016/J.CIRP.2013.03.051.

[25] Piccininni A, Palumbo G, Franco A Lo, Sorgente D, Tricarico L, Russello G. Multi objective genetic algorithm to optimize the local heat treatment of a hardenable aluminum alloy. AIP Conf Proc 2018;1960. https://doi.org/10.1063/1.5034965/886693.

[26] Merklein M, Nguyen H. Advanced laser heat treatment with respect for the application for Tailored Heat Treated Blanks. Phys Procedia, vol. 5, Elsevier B.V.; 2010, p. 233–42. https://doi.org/10.1016/j.phpro.2010.08.049.

[27] Reuther F, Lieber T, Heidrich J, Kräusel V. Numerical investigations on thermal forming limit testing with local inductive heating for hot forming of aa7075. Materials 2021;14. https://doi.org/10.3390/ma14081882.

[28] Nishiwaki T, Sako R, Tsutamori H. Hydro-Mechanical Deep Drawing of Locally Solution-Treated Aluminum Alloy Sheets. In: Daehn G, Cao J, Kinsey B, Tekkaya E, Vivek A, Yoshida Y, editors. Forming the Future, Cham: Springer International Publishing; 2021, p. 2729–39.

[29] Rigas N, Merklein M. Numerical and experimental investigations for distortion-reduced laser heat treatment of aluminum. Production Engineering 2021;15:479–88. https://doi.org/10.1007/s11740-021-01029-3.

[30] Bianco N, Manca O, Nardini S, Tamburino S. Transient heat conduction in solids irradiated by a moving heat source. Defect and Diffusion Forum, vol. 283–286, Trans Tech Publications Ltd; 2009, p. 358–63. https://doi.org/10.4028/www.scientific.net/DDF.283-286.358.

[31] Bruschi S, Altan T, Banabic D, Bariani PF, Brosius A, Cao J, et al. Testing and modelling of material behaviour and formability in sheet metal forming. CIRP Ann Manuf Technol 2014;63:727–49. https://doi.org/10.1016/j.cirp.2014.05.005.

[32] Lechner M, Johannes M, Kuppert A, Merklein M. Influence of pre-straining and heat treatment on the yield surface of precipitation hardenable aluminum alloys. Phys Procedia, vol. 56, Elsevier B.V.; 2014, p. 1400–9. https://doi.org/10.1016/j.phpro.2014.08.070.

[33] Piccininni A, Palumbo G. Numerical modelling of the annealing determined by short-term laser treatment using a physical simulation-based approach. CIRP J Manuf Sci Technol 2023;45:210–24. https://doi.org/10.1016/j.cirpj.2023.07.006.

[34] Pereira R, Peixinho N, Costa SL, Blanco V, Carneiro V, Cortez S. Parametric study of local laser heat treatment technology on multi forming of advanced-high strength steel (AHSS) part with complex shape. International Journal of Lightweight Materials and Manufacture 2024;7:248–59. https://doi.org/10.1016/J.IJLMM.2023.10.002.

[35] Piccininni A, Palumbo G. Design and optimization of the local laser treatment to improve the formability of age hardenable aluminium alloys. Materials 2020;13. https://doi.org/10.3390/ma13071576.

[36] Fröck H, Graser M, Reich M, Lechner M, Merklein M, Kessler O. Numerical modelling of the process chain for aluminium Tailored Heat-Treated Profiles. Adv Model Simul Eng Sci 2023;10:1–18. https://doi.org/10.1186/S40323-023-00247-X/FIGURES/21.

[37] Lattanzi A, Piccininni A, Guglielmi P, Rossi M, Palumbo G. A fast methodology for the accurate characterization and simulation of laser heat treated blanks. Int J Mech Sci 2021;192. https://doi.org/10.1016/j.ijmecsci.2020.106134.

[38] Cusanno A, Moturu S, Carty D, Palumbo G. Influence of the laser heat treatment on the AA5754-H32 strain path during hydraulic bulge tests. ESAFORM 2021 - 24th International Conference on Material Forming, 2021. https://doi.org/10.25518/esaform21.1536.

[39] A. Piccininni, G. Palumbo ALF. Numerical Simulation of the Stamping Process of an AA5754 Railway Vehicle Component using a Locally Annealed Blank. Conference Proceeding NUMIFORM 2019 n.d.

[40] El Fakir O, Wang L, Balint D, Dear JP, Lin J, Dean TA. Numerical study of the solution heat treatment, forming, and in-die quenching (HFQ) process on AA5754. Int J Mach Tools Manuf 2014;87:39–48. https://doi.org/10.1016/j.ijmachtools.2014.07.008.

[41] Lattanzi A, Piccininni A, Guglielmi P, Rossi M, Palumbo G. A fast methodology for the accurate characterization and simulation of laser heat treated blanks. Int J Mech Sci 2021;192. https://doi.org/10.1016/j.ijmecsci.2020.106134.

Highlights of the manuscript:

- A novel methodology for influencing the strain paths during hydraulic bulge tests was proposed;
- The methodology involves laser heat treatments in specific areas before the test;
- The laser heat treatment was designed by a numerical/experimental approach;
- Experimental tests were conducted to validate the proposed methodology.

Declaration of interests

☒ The authors declare that they have no known competing financial interests or personal relationships that could have appeared to influence the work reported in this paper.

☐ The authors declare the following financial interests/personal relationships which may be considered as potential competing interests: